

Quantified Marine Oil Emissions with a Video-Monitored, Oil Seep-Tent

AUTHORS

Ira Leifer

University of California, Santa Barbara
Engineering Research Center

Ken Wilson

California Department of Fish and Game,
Oil Spill Prevention and Response

ABSTRACT

A video-monitored oil capture tent was developed and deployed during two field trips to quantify oil emissions from several sites in nearshore waters off Summerland Beach in Santa Barbara County, California, at a water depth of ~5 m. The tent was a tall, inverted polyvinyl chloride plastic cone, which funneled oil into a video-observed sample collection jar. Sample jars were periodically retrieved and analyzed to determine oil and gas emissions at two seeps not associated with physical structures, and a suspected abandoned oil well, designated S-3. Oil and gas emissions at the seeps were ~1 ml day⁻¹ and ~90 L day⁻¹, respectively. At the S-3 site, emissions were 51 ml oil day⁻¹ and 0.35 L gas day⁻¹. The size distribution of bubbles at S-3 was sharply peaked at 1500- μ m radius, and bubbles rose significantly slower than equivalent size non-oily bubbles, demonstrating the effect of oil on buoyancy loss. A method was developed to estimate from the measured rise velocities the oil-to-gas ratio of each bubble, calibrated with the sample analysis oil and gas fluxes. Autocorrelation showed strong peaks at 64.3 s and 120.0 s period, which were likely related. Other autocorrelation peaks at multiples of 8.2 s corresponded to Fourier spectrum peaks at 8 s and 23.4 s, and were proposed to relate to wave swell-induced surge. Other spectral peaks were observed at 4.9 s, 13.0 s, and 45-50 s period.

INTRODUCTION

1.1. Motivation

Petroleum in the ocean is of enormous concern, affecting the environment, economy, and quality of life for coastal inhabitants. Globally, 1,300,000 tons of oil entered the oceans annually in the 1990s, of which natural seeps emitted 600,000 tons. Tank vessel spills accounted for 100,000 tons, run-off 140,000 tons, while pipelines just 12,000 tons. A total of 160,000 tons of oil are emitted annually from seeps in North America. California seeps annually emit 20,000 tons of oil, ~12% of the North American total (NRC, 2003). Despite the significance of oil in the ocean, many aspects of its fate remain poorly understood.

Natural seeps long have aided oil prospectors in determining where to conduct geotechnical surveys, build piers, drill wells, and place platforms. Much of the California coastline, from Pt. Conception to Santa Monica, was home to numerous oil piers, platforms, and wells in the nearshore and offshore waters, many of which are now abandoned. A number of

these oil facilities were alleged to have been improperly abandoned, posing a threat of leakage (Grosbard, 2002). Facilities located in natural seepage areas, such as offshore Summerland Beach, California (USCG, 1995; PENCO, 1995), provide a particular challenge with respect to discriminating between natural and anthropogenic oil emissions. This is particularly relevant in cases where the responsible parties no longer exist and state and/or federal taxpayers are asked to pay for control, containment, and cleanup.

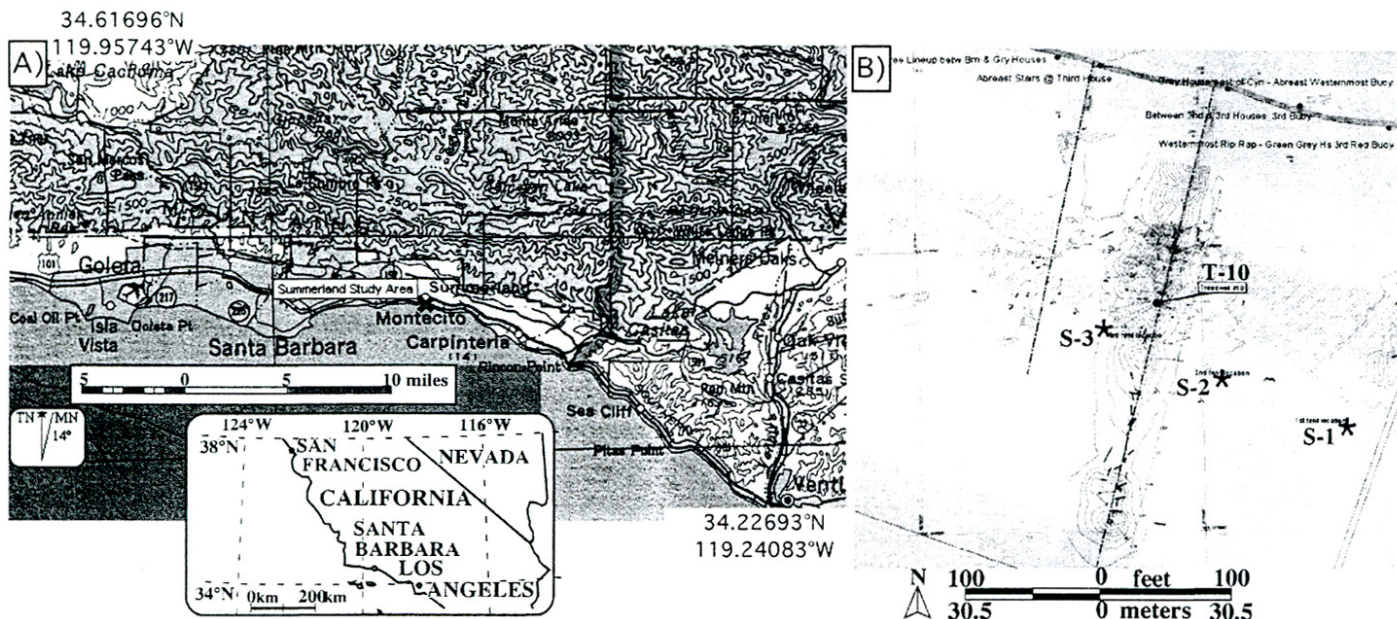
Identifying and quantifying sources of oil and seabed emissions are the first steps in assessing the need for and desirability of various mitigation strategies. However, absent understanding the causes of variability in emissions from both anthropogenic and natural sources, accurate assessment can be elusive. Temporal and spatial variability in seabed oil emissions influence the location and appearance of surface slicks and the disposition of the newly surfaced oil. In this paper, we present a new technique for quantifying seabed emissions—a

diver-deployed, video-monitored oil seep-tent, that provided both real-time and high time-resolution monitoring of oil emissions, allowing assessment of variability. Absent long-term, *in situ* monitoring, which can be expensive, assessment of sources of variability is key to determining if flux measurements during any given interval represent upper limits.

In an effort to identify and quantify the source(s) and intermittency of oil emissions in the Summerland Beach area, dive and beach studies were conducted to locate the Treadwell-10 Well (T-10) site and other emission sites. Studies included deployment of oil-capture seep-tents to quantify gas and oil emissions. These studies also sought to understand the magnitude of the effects on beaches and wildlife. While the field studies were directed primarily at abandoned oil wells in shallow (5.2 m) nearshore waters off Summerland, California, the methods and conclusions are also applicable to natural seepage and abandoned oil wells elsewhere in the marine environment.

FIGURE 1

A) Map of area surrounding Summerland study area (from Topo! 1997 Wildflower Productions). GPS coordinates are NAD83. Inset: Map of S. California.
B) Summerland study area map (Golder Associates, 1995) with seafloor bathymetry (contours in feet). S-1 to S-3 are tent deployment sites, and T-10 is the proposed location of the abandoned Treadwell-10 well.



1.2. Background

Onshore, nearshore, and offshore oil seeps have attracted prospectors since the late 1800s (Grosbard, 2002). The world's first offshore well was drilled in Summerland (Giallonardo and Koller, 1978). The field was depleted and production ceased circa 1906. Abandonment procedures for depleted oil wells left much to be desired. For example, depleted oil wells at Summerland were often stuffed with "... rags, rocks, earth and wooden poles ..." (Fairweather Pacific, 2000). Despite multiple efforts to re-abandon the T-10 and other wells (Lammers, 1975; Curran, 1995), reports of leakage persist (Fairweather Pacific, 2000). Leakage occurs (1) through the process of natural seepage, in which oil and gas are driven through fractures primarily along faults from the reservoir source to the surface, and (2) along low resistance pathways associated with abandoned oil wells. One such area, located offshore Summerland Beach in 5.2-m water (see Fig. 1), is an example of where both may be occurring. Natural seepage (Freckman, 1981; Curran, 1995; USCG, 1995) and oil from some abandoned wells (PENCO, 1994) have been reported to contribute to oiled beaches and surface waters at Summerland.

Over the years, reports of petroleum sheens (beach and sea surface) in the Summerland area have been attributed to leakage from the T-10 site; however, the reports have been inconsistent (Fairweather Pacific, 2000; Leifer et al., 2004). This may be due to intermittency and variability of the emissions from the T-10 site, other anthropogenic sources, and/or natural sources. There also have been reports of oil emissions from the intertidal zone. The first estimate, reported by the U.S. Coast Guard (USCG) in 1994, was ~ 21 L day⁻¹ (1/2 barrel day⁻¹) from the vicinity of an abandoned oil facility, Becker Onshore (USCG, 1995). A more recent estimate at the same site was 12 L day⁻¹ through a thick sand overburden (Leifer et al., 2004).

2.0. Seep Tents

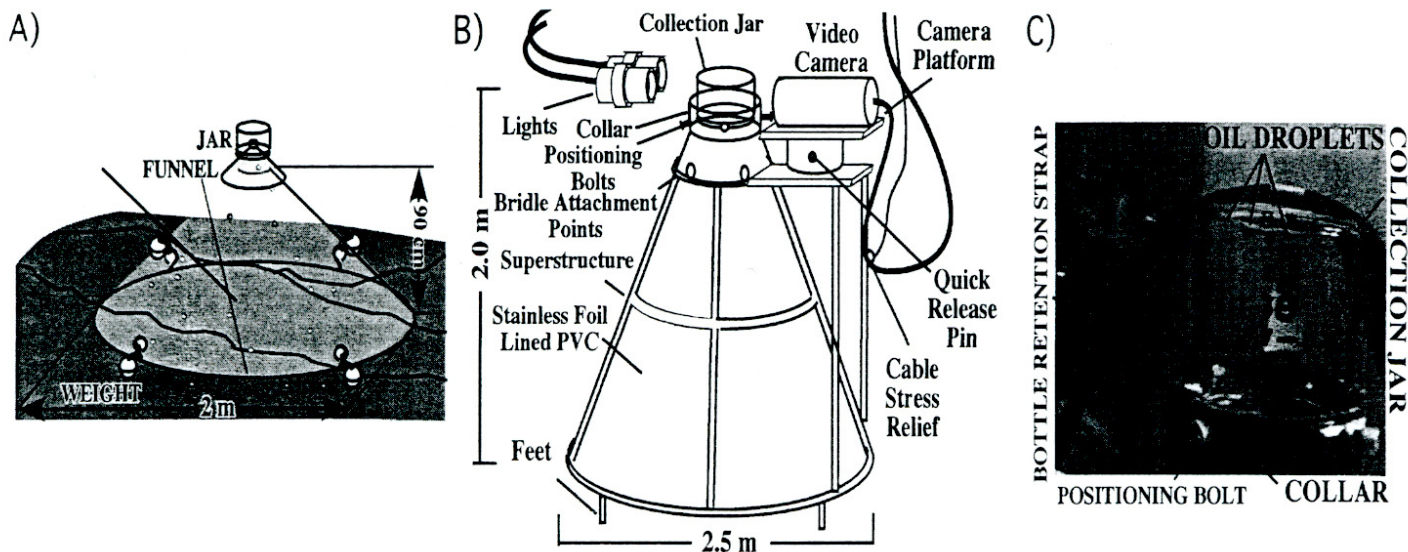
Seep tents of two different designs were deployed in nearshore waters off Summerland in two separate operations, the first in May 2003 and the second in October 2003. In May 2003 a modified, gas seep-tent was deployed to collect oil and gas. The tent was the base of a turbine seep-tent (Leifer and Boles, 2004b) absent the turbine (Fig. 2A). The tent was a 1 m tall cone with a 2 m base diameter

constructed from 1/16 inch thick sheets of polyvinyl chloride (PVC) plastic, pop riveted together. The cone was riveted to a support frame of 1/2-inch diameter PVC pipes. The bottom of the support frame was a PVC pipe ring that was attached to the tent plastic by a rope threaded through a series of holes at the tent's bottom edge. A deployment bridle was attached to three eyebolts in the frame. This configuration evenly distributes stress during recovery, when the tent acts like a sea anchor. Five 2 kg diving weights were connected to the frame to keep the tent on the seabed despite the swell. An inverted glass jar held above a stainless steel funnel collected oil and gas. Periodically, a diver retrieved, capped, and replaced the jar with a new one.

An improved second oil seep-tent was designed and constructed and is shown schematically in Fig. 2B. The new tent profile was significantly steeper to reduce the likelihood of oil attachment to the tent's inner surface thereby preventing capture by the collection jars. The new tent was wider and thus taller (2.5 m diameter and 2 m tall) to increase the collection area. This tent was made of 1/16 inch PVC sheeting, pop riveted together, and its interior surface was lined with aluminum foil. The tent had a 1"

FIGURE 2

A) First oil seep tent. B) Second oil seep tent and C) Image of oily bubbles entering collection jar on second oil seep tent.



diameter PVC-pipe framework, which provided support and attachments for stability weights, bridle hook-ups, and feet. Feet outfitted to the framework held the tent above the seabed, reducing the tendency of swell and tent movements to disturb and release oil from oil-saturated sediment below the tent's edge. The PVC-pipe framework had holes drilled to allow water to enter during deployment, reducing the tent buoyancy.

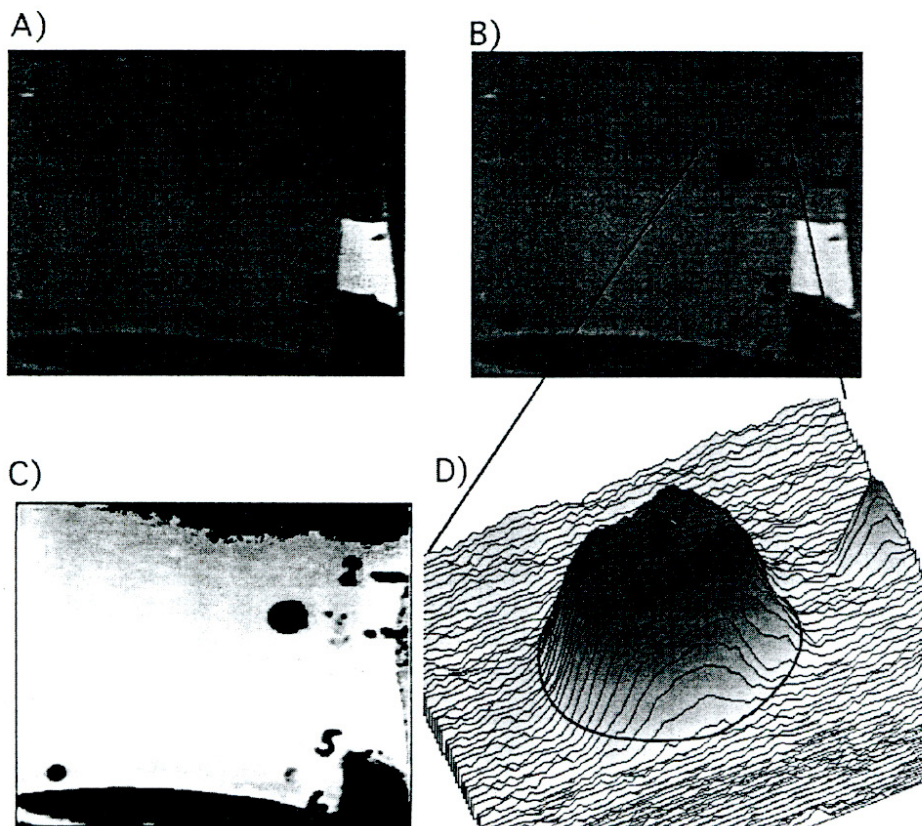
A clear, 200 ml, wide mouth glass collection jar mounted over the cone's narrow end collected gas and oil (Fig. 2C). The jar sat on the rim of a cut stainless-steel funnel mounted in the top of the tent. The cutoff funnel opening was several millimeters narrower than the jar opening. Six bolts threaded into a collar positioned the jar. A quick release strap allowed easy exchange by divers. Jars were numbered and marked every 1 cm for a video size-scale. A video camera (SuperCam 6500, DeepSea Power and Light, San Diego, CA) transmitted images of the jar to a shipboard video recorder. The camera was mounted on a plate with an attached PVC pipe that was tightly inserted into a larger PVC pipe mounted on a platform secured to the tent framework. A quick-release pin secured the camera to the mount. Two undersea, AC powered lights backlit the jar and its contents, overpowering the ambient light (Leifer and MacDonald, 2003). The lights also allowed

nighttime operation. The video camera was remotely controllable, allowing selection of a

sufficiently fast shutter speed to prevent motion blurring (Leifer et al., 2003a).

FIGURE 3

Example of image analysis procedure for a 4770 μm radius bubble with a thick oil coating rising in the collection jar. A. Original image. B. Extracted image. C. Thresholded image. D. Two-dimensional intensity profile of image subset indicated by dashed box on B.



3.0. Video Analysis

Analysis of the video provided high time-resolution bubble emission series allowing calculation of the oil and gas transported by each oily bubble. Video was digitized into a series of frames (108,000 hr⁻¹). Navigation through the sequence of files, image processing, and basic analysis was performed with routines written in NIH Image (National Institute of Health, 2003). Since most frames were empty, only a small percentage required analysis. Moreover, since the oily bubbles rose slowly, bubbles were analyzed for each five frames in the sequence. This allowed a statistically significant number of measurements of each oily bubble to account for shape oscillations and noise. Frames with bubbles (Fig. 3A) were “extracted” (Fig. 3B), a process in which each odd pixel row is replaced by interpolation of neighboring even pixel rows (Leifer et al., 2003a). Extraction removes interlacing effects. The image was then thresholded—i.e., made binary (Fig. 3C)—at an intensity slightly above the background. Correctly choosing the intensity threshold was important since the measured bubble diameter decreases with increasing thresholding intensity. This can be seen in the cone shape of the 2-dimensional intensity surface plot (Fig. 3D). The threshold value used in Fig. 3C is indicated in Fig. 3D by a line. Leifer et al. (2003b) showed that the appropriate intensity is slightly below the background, because bubbles are surrounded by a bright halo created by off-axis reflected rays.

From this analysis, a time series of major and minor axes and x and y locations was produced. Since the units were pixels per frame (at 30 frames per second), a size scale and the frame rate were used to convert to cm s⁻¹. The variable length lens was set at ‘wide angle’ because poor water visibility prevented obtaining clear images unless the camera was very close to the collection jar. Thus, the size scale varied significantly from 32 pixels cm⁻¹ at the distant jar wall, to 48 pixels cm⁻¹, at the jar’s near wall. This size uncertainty was minimized by noting whether oily bubbles were in the near, center, or distant portion of the jar and us-

ing the appropriate size scale. In this manner, size error was reduced to about ±7%. Further analysis was by routines written in MatLab (The Mathworks, Mass).

The bubble equivalent spherical radius, r , was

$$(1) \quad r = \sqrt[3]{r_1^2 r_2}$$

where r_1 was the major radius, and r_2 was the minor radius (Sam et al., 1996). Each bubble was tracked through the frame sequence, and measurements of r and V_B for each bubble were averaged together. The bubble rise velocity, V_B , was calculated from the vertical distance between bubble locations in subsequent frames.

The bubble size-distribution, Φ , was determined by size segregating the time series of radii into logarithmically spaced bins and normalizing to per unit radius increment and per time interval (i.e., the number of seconds analyzed). Error bars were calculated from the square root of the number of bubbles in each radius bin. Bubble size-distributions generally are described by a power law dependency—e.g., Johnson and Cooke (1979),

$$(2) \quad \Phi(r) = k r^{-S}$$

where S is the power law exponent and k is a constant. Values of S were calculated by a least-squares, linear-regression analysis of the log of both sides of (2) over an appropriate size range.

Bubble sizes within the camera field of view were larger than at the seabed due to the decrease in hydrostatic pressure. Seabed depth was 5.2 m while the camera was at a depth of 3.2 m. Thus, by Boyle’s law, $P_1 V_1 = P_2 V_2$. Using the volume of a sphere, yields $r_2 = r_1 (P_1/P_2)^{0.33}$. For $P_1 = 1.32$ Atm and $P_2 = 1.52$ Atm, the increase in bubble size from the seabed to collection jar was 4.8%. This is an upper limit because some fraction of the bubble volume was incompressible oil. A second factor that could cause bubble growth is oil outgassing. Absent data on the dissolved gas pressure in the oil, we assumed that the gas and oil were in equilibrium at the seabed.

Oil has the effect of decreasing a bubble’s buoyancy. Thus, comparison of the measured V_B with V_B for similar sized, oil-free bubbles allows the amount of oil on each bubble to be inferred. For this approach it is necessary to know whether the comparison is with an oil-free, clean bubble or an oil-free, dirty bubble. Herein, clean and dirty refer to hydrodynamic behavior. Dirty bubbles are contaminated with surfactants (surface-active substances), which are compounds or particles that have both hydrophobic and hydrophilic sites, i.e., they “prefer” air-water interfaces. Dirty bubbles rise slower and exchange gas slower than clean bubbles. A bubble can be hydrodynamically clean in contaminated water if insufficient surfactant has accumulated on the bubble surface (Leifer and Patro, 2002). For example, Patro et al. (2002) showed that bubbles larger than $r = 1500$ μm behaved clean in seawater. For this analysis, we propose that since oil is surface active, the behavior of an oily bubble, absent its buoyancy effects, is most like a hydrodynamically dirty bubble. Thus, we propose the appropriate comparison is between the measured V_B and V_B for dirty bubbles.

The bubble V_B is a balance between the drag and buoyancy forces, where the buoyancy force is driven by the density difference between the water and the oily bubble. There is no simple expression for the drag force, except for very small and slow rising bubbles where the flow around the bubble is laminar ($Re < 1$, where Re is the non-dimensional Reynolds number and is defined $Re = 2rV_B/\nu$ where ν is the kinematic viscosity of water). At higher Re , details of the bubble’s wake and bubble shape are important. To estimate the oil mass on the bubble, we looked at the decrease in rise velocity due to decreased buoyancy. Buoyancy affects V_B by the density difference between the water and the oily bubble, and is expressed for laminar flow bubbles ($Re < 1$) by Stoke’s rise velocity, V_{B-ST} , which is (Clift et al., 1978)

$$(3) \quad V_{B-ST} = \frac{2}{9} \frac{gr^2}{\nu} (\rho_w - \rho_B)$$

where g is gravity, ρ_w is water density, ρ_B is the bubble density. For a pure gas bubble,

$\rho_w \gg \rho_B$ and is $(\rho_w - \rho_B) \sim 1$, although with increasing oiliness, ρ_B increases and $\rho_w - \rho_B$ decreases. Equation (3) can be solved for ρ_B and then using the bubble volume ($4/3 \pi r^3$), the bubble mass, M_B , (both oil and gas) can be calculated if the oil density is known. The problem with using Stokes V_B is that it is inappropriate for the bubbles observed which had large values of Re . Instead, we solved for M_B using the ratio of observed and predicted $V_B(r)$ —dirty, non-oily. The empirical parameterization for dirty V_B is shown in Fig. 7. We assumed that oil-coated bubbles behaved hydrodynamically dirty (Leifer and Boles, 2004a). Based on Equation (3), we related the ratio of density differences to the ratio of the rise velocities,

$$(4) \frac{V_B}{V_{B-Dirty}} = k \frac{(\rho_w - \rho_B)}{\rho_w}$$

where k is a function of radius that describes the effect of oil on bubble hydrodynamics. Specifically, as the oil decreases buoyancy and decelerates the bubble, the drag also decreases. Consequently, the bubble does not slow down as much as if the drag had not decreased—i.e., the reduction in V_B is less if the effect of oil on bubble hydrodynamics is included. For Stoke's rise, $k = 1$, but for higher Re , $k < 1$. In Equation (4) the bubble density for the non-oily dirty V_B is much less than ρ_w and was neglected. Equation (4) can be solved for ρ_B , which is simply M_B divided by its volume,

$$(5) \frac{\rho_w}{k} \left(1 - \frac{V_B}{V_{B-Dirty}}\right) = \frac{3M_B}{4\pi r^3}$$

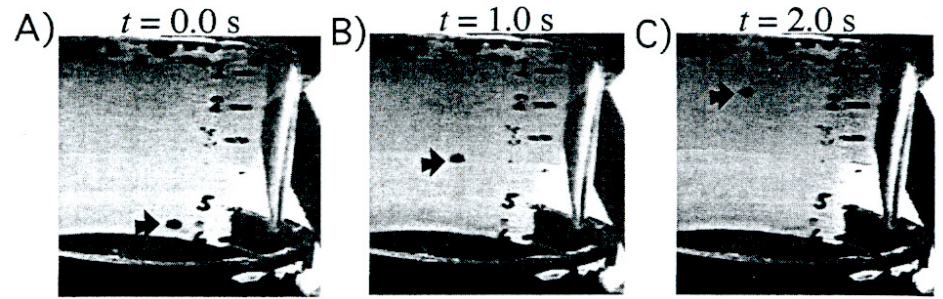
or

$$(6) M_B = \frac{4\pi r^3 \rho_w}{3k} \left(1 - \frac{V_B}{V_{B-Dirty}}\right)$$

Once the oil volume is determined using the oil density, $\rho_{oil} \sim 0.975 \text{ g cm}^{-3}$ for reservoir oil in the Summerland area (Bill Castle, California Dept. of Fish and Game, Office of Spill Prevention and Response (OSPR), personal communication, 2004), the gas volume, Vol_{GAS} is calculated by subtracting the oil volume, Vol_{OIL} , from the bubble volume, Vol_B .

FIGURE 4

Image sequence of a $4770 \pm 250 \mu\text{m}$ radius oily bubble rising in the collection jar. Time relative to first panel, t , noted above each panel; horizontal lines are 1 cm apart. The drop rose at 2.8 cm s^{-1} , and had a Reynolds number of 250. Arrow indicates position of bubble.



$$(7) Vol_{GAS} = Vol_B - Vol_{OIL} \\ = \frac{4\pi r^3}{3} - \frac{M_B}{\rho_{OIL}}$$

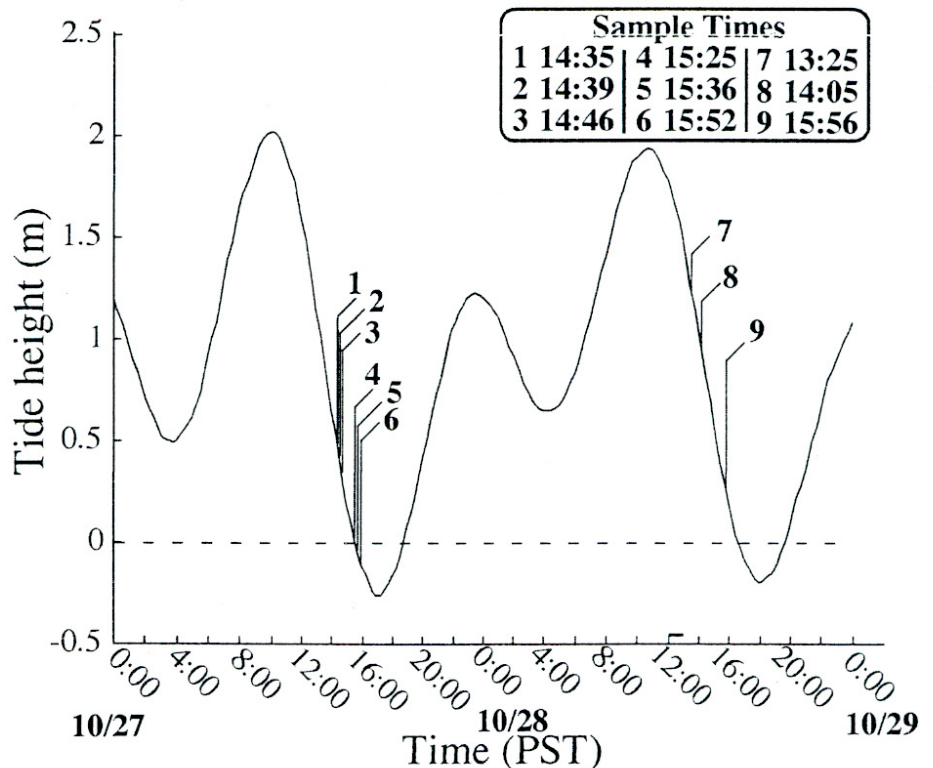
An example image sequence is shown in Fig. 4. The bubble had $r = 4770 \mu\text{m}$ and $V_B = 2.8 \text{ cm s}^{-1}$. In comparison, $V_{B-Dirty} = 20 \text{ cm s}^{-1}$, thus its V_B ratio was 0.136. Using Equation (6) with $k = 1$ yielded $M_B = 0.4 \text{ g}$ for a 0.455 cm^3 bubble. The gas volume from Equation (7) was 0.54 cm^3 and the oil to gas volume ratio for this oily bubble was

7.4 to 1, implying this bubble was primarily an oil droplet containing a small gas bubble. Since the observed oil to gas ratio for this jar was 1 to 5.3, either this bubble was highly atypical, the assumption $k = 1$ was inappropriate, or both. With regard to whether the bubble was atypical, it had a V_B ratio significantly less than for other similar size bubbles.

The approach outlined above assumes the effect of oil on the rise of a bubble is solely due to buoyancy ($k = 1$), neglecting

FIGURE 5

Tide height at Summerland for Oct 27-28, 2003.



hydrodynamic effects. If hydrodynamic effects were included, the reduction in V_B would be less ($k < 1$), thus, M_B is an upper limit. The authors are unaware of any literature on oily bubble hydrodynamics. Thus, the value for k was derived by summing M_B for all bubbles that entered the jar and dividing by the measured oil in the jar. This represents a first step, and must neglect factors upon which k depends—i.e., factors that affect bubble hydrodynamics such as radius, oiliness, and temperature.

4.0. Results

4.1. Field Observations and Tent Deployments

Field deployments were scheduled for periods of a minus tide. On May 20, 2003, the modified gas seep-tent (Fig 2A) was deployed in 5.2 m of water on a flat sandy seabed with a sand overburden of undetermined thickness, in nearshore waters off Summerland, CA. Divers noted droplets and stringers of oil and gas bubbles emerging from holes in the sandy bottom, and surface slicks originating from the region. The tents were deployed for 20 minutes and the collected gas to oil ratio was estimated at 100 to 1 (analysis by the OSPR's Petroleum Chemistry Laboratory) with total estimated oil seepage of ~ 36 ml day⁻¹ for the entire area surrounding the tent. Uncertainty in the number arises from a poorly constrained seabed seepage area.

On Oct. 27-28, 2004, divers positioned the oil seep-tent (Fig. 2B) at three seepage sites. Deployments were planned to coincide with significant minus tides (Fig. 5). The measurements are summarized in Table 1. The first site, Site 1, was located on a featureless sandy bottom, similar to the deployment site of May 20, 2003. Seep bubbles appeared clear and the measured gas to oil ratio was $111,000 \pm 55,000$ to 1, with estimated gas seepage of 90.4 ± 14 L day⁻¹ for the area covered by the tent. Clearly, these bubbles were very slightly oily. The oil emission rate was 0.98 ml day⁻¹ for the area covered by the tents. Bubbles at the second site (Site 2) were similar in appearance to site 1 bubbles as was the measured gas-to-oil ra-

tio, $94,000 \pm 20,000$ to 1. Estimated daily oil and gas seepage rates for the area covered by the tents were 1.07 ± 0.4 ml day⁻¹ and 96.2 ± 21 L day⁻¹, respectively.

At the third site (Site 3, S-3), most bubbles appeared black, and there was the most significant number and extent of sea-surface oil slicks off Summerland at this site. The seabed consisted of sand, cobbles, subcanopy forming algae, and the ornate tubeworm, *Diopatra ornata*. A partially buried concrete cap and metal form was found, and the site was designated S-3. The site was located ~ 30 m southwest of the California State Lands Commission (CSLC) coordinates for the T-10 Well. The measured gas-to-oil ratio at this location was 8.36 ± 6.9 to 1. Gas and oil seepage was very different from the other sites. Gas seepage was 350 ± 330 ml day⁻¹, oil seepage was 51.5 ± 65.5 ml day⁻¹. The large variability arose from an increase by an order of magnitude in both oil and gas emissions for the last of the three samples collected at S-3 (See Table 1).

While seabed observations at S-3 suggested seabed emissions primarily arose from a 4 m diameter area, the surfacing footprint of oily bubbles suggested a larger seabed emission area, ~ 8 m diameter. Based on the observed 47 ml day⁻¹ and 6% tent coverage, the daily site emission rate was 0.8 L day⁻¹. Underwater visibility in this extremely shallow water was very poor during all surveys. Thus, the seabed area estimate was qualitative, but likely conservative.

4.2. Video Observations

4.2.1. Bubble Distribution

Φ for oily bubbles showed a sharp peak (Fig. 6). The distribution was narrowly peaked, which is typical for low flow vents where bubbles escape singly or in bubble lines (Leifer and Boles, 2004a). Values smaller than $r \sim 1000$ μm were unreliably close to the lower size limit. The power law exponent, S , was 3.84, i.e., Φ decreased sharply. Because $S > 3$, the maximum in the bubble volume was close to the peak in Φ .

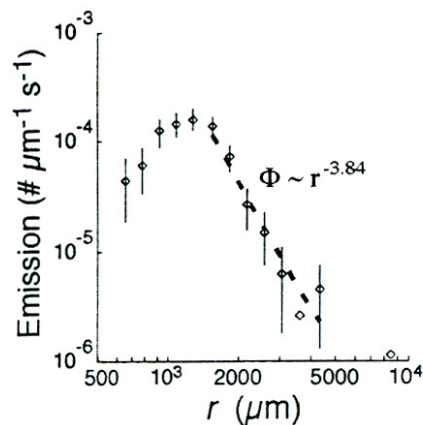
TABLE 1

Results of analysis of collected sample jars for oil and gas. Coordinates in NAD 27

Sample	Time deploy	Time (min)	Oil (ml)	Oil Flux (ml dy ⁻¹)	Gas (ml)	Gas Flux (L dy ⁻¹)	Gas/Oil ratio
Site 1, 10/27/2004			34.4175858°N, 119.5969998°W				
1	14:35	5.15	0.0027	0.75	364.60	101.95	135,000
2	14:39	6.20	0.0027	0.63	407.70	94.69	151,000
3	14:46	5.00	0.0054	1.56	259.40	74.71	48,000
Site 2, 10/27/2004			34.4178164°N, 119.5977455°W				
4	15:25	6.32	0.0027	0.62	318.50	72.57	117,000
5	15:36	4.08	0.0036	1.27	298.70	105.42	83,000
6	15:52	3.46	0.0032	1.33	265.30	110.41	82,900
Site 3, 10/28/2004			34.4180579°N, 119.5984375°W				
7	13:34	31.3	0.4910	22.6	8.00	0.368	16.3
8	14:05	112.29	0.4310	5.53	1.50	0.019	3.48
9	15:56	26.60	2.3360	126.46	12.40	0.67	5.31
Mean Site Values			Oil Flux (ml day⁻¹)	Gas Flux (L day⁻¹)			
Site 1			0.979±0.4	90.4±14			
Site 2			1.072±0.4	96.2±20			
Site 3			51.5±65.5	0.35±0.33			

FIGURE 6

Oily bubble emission size-distribution as a function of radius, r , of all analyzed oily bubbles and fit to data over size range shown.



In contrast, Leifer and Boles (2004a) found that Φ for high flow rate vents (where bubbles come out in a plume rather than singly or in lines) were very different, both broad and shallow. The different shape of Φ was primarily due to bubble breakup both at the vent mouth and in the rising bubble stream due to turbulence. For the low emission vents observed at Summerland, bubble breakup did not occur. Furthermore, the presence of thick oil coatings may play a roll in stabilizing bubbles against breakup.

At these low emission rates, the bubble size is determined solely by vent diameter (Blanchard and Syzdek, 1977). In this case, the vent mouth was most likely the sand pore-throat diameter. Based on observations of seeps at Coal Oil Point, CA, Leifer and Boles (2004a) proposed that time-varying oil emissions create an oil coating of varying thickness on the vent mouth (and walls) and thereby cause the bubble size to vary.

4.2.2. Rise Velocity

Confirmation of the oil analysis conclusion that bubbles were heavily oil contaminated is shown by a plot of V_B versus r for the analyzed bubbles (Fig. 7). V_B was significantly slower than the dirty (non-oily) V_B parameterization; however, the general data trend roughly followed the dirty parameterization. For example, there was no peak in $V_B(r)$ as there is for the clean V_B parameterization. There was a roll-off for small bubbles at $r \sim 1500 \mu\text{m}$, which is similar to the roll-off in the dirty V_B parameterization at $r \sim 1000 \mu\text{m}$. A second-order polynomial was fit to the V_B values with a least-squares, linear-regression analysis and was:

$$(8) V_B = 1.29 + 0.0025 r - 1.04 \times 10^{-7} r^2$$

which had a finite velocity (1.29 cm s^{-1}) for a zero-radius bubble, indicating the difficulty

of forming very small oily bubbles. For the data shown in Fig. 7A, Re varied between ~ 20 and 104 , i.e., Re for these bubbles were too large for Stoke's V_B to have been appropriate.

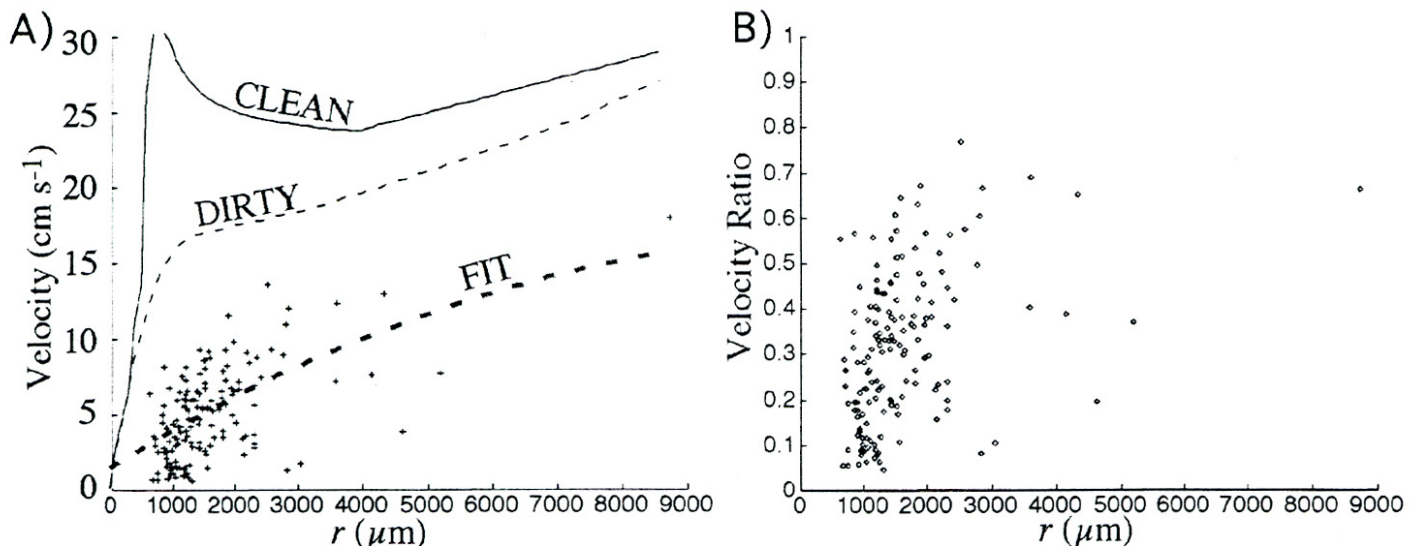
Bubbles from natural hydrocarbon seeps escape with varying oil to gas ratios (Leifer and Boles, 2004a), and the same was true for emissions at the S-3 site. This is shown by the scatter in $V_B(r)$, up to a factor of three (Fig. 7A) and the variation in the velocity ratio $V_B/V_{B-Dirty}$ from 4.7% to as high as 77% (Fig. 7B). Larger bubbles generally had the highest gas-to-oil ratios, although some small bubbles had very high ratios, too. The mean velocity ratio was $32 \pm 17\%$. Since the velocity ratio varied significantly at a given r , the oil-to-gas ratio must have varied from bubble to bubble. Furthermore, since the analysis did not show significant non-petroleum detritus, hydrocarbons must have caused the buoyancy reduction.

4.2.3. Oil and Gas Volume Emission

Using the approach outlined above, the oil and gas fluxes were estimated for the analyzed video and compared with the quantitative values shown in Table 1 to test the $k = 1$ assumption. Since only a 10-minute video sequence ($\sim 20,000$ frames) was analyzed, the calculated flux rates were scaled to the collection time for the sample

FIGURE 7

A) Bubble vertical rise velocity, V_B , versus radius, r , and fit to data over size range shown. Also shown are the clean and dirty (non-oily) bubble V_B parameterizations in stagnant water from Clift et al. (1978) and polynomial, least-squares fit to the data. B) Ratio of V_B to dirty V_B parameterization with respect to r .



jars. Thus, we assumed that Φ remained approximately constant during the collection period. From the bubble video analysis, the total predicted oil flux for sample jar 8 was 37 mg oil compared with 0.43 ml oil, yielding $k = 0.016$, i.e., $k \ll 1$. Using $k = 0.016$, the oil flux time series was calculated and is shown in Fig. 8A, where the mass of all bubbles in each 2-second time bins was summed and then normalized to units of mass per second. A significant amount of the mass occurred in a single pulse at -375 s; although there were two smaller, but significant pulses at -125 s and

-275 s. There also appears to be several series of smaller pulses involving numerous bubbles lasting 10-15 seconds—e.g., at 305 s. Of greater interest than the arrival time at the collection jar is the seabed emission time series, shown in Fig. 8B. The seabed emission time was calculated using the tent height and the rise speed of each bubble. We define the oil “flux” as in the water column, while emission is solely at the seabed. Interestingly, the three largest pulses were emitted in evenly spaced intervals of -120 s, while the smaller pulses appear less organized.

The series was then smoothed with a low-pass filter (Fig. 8C) and detrended to allow calculation of the spectrum. An autocorrelation was calculated for the smoothed, detrended data series (Fig. 9A). There were two clear peaks at 64.3 s and 120.0 s for the detrended data, matching the significant peaks in Fig. 8C. A spectrum for the data series (not shown) showed a significant peak at 120 s, and numerous harmonics due to the data's delta function-time character. Thus, the three main peaks in Fig. 8C were deleted (Fig. 8D) and the autocorrelation and spectrum (Fig. 9B) recalculated. The strongest peaks were at 105 s, 49.2, 8.2 s, with decreasing peaks at 16.0 and 25.0 s that are integer multiples of a strong peak at 8.2 s. The smoothed time series was detrended and a 256-point Fourier transform with 50% overlap and a Blackman window performed (Fig. 9C).

There were strong peaks at 8.0, 13.0, and 23.4 s as well as a very sharp peak at 4.9 s and a broad peak at 45 – 55 s (Fig. 9C). The 8 and 23.4 s peaks likely were harmonics, as may be the shoulder of the 13.0 s peak, at -15.0 s. The 8 s period peak, also observed in the autocorrelation, was similar to the wave period observed at the site (5 – 8 s) in video of wave-induced surge. Swell during this field study (Oct 27-28, 2003) was very weak, ~ 10 cm; however, underwater video showed surge motions moving detritus back and forth. This surge may also explain the narrow 5 s peak. Other peaks may relate to details of the subsurface oil flux, akin to the dripping of water from a leaky faucet.

FIGURE 8

A) Time series of oil flux at collection jar at site S-3; zero time is arbitrary. **B)** Time series of oil seabed emission, corrected to seabed emission time; zero time is relative to **A**. **C)** Smoothed time series of seabed oil emissions. **D)** Same as **C**, but with three main peaks deleted. Note time scale on **B**. - **D**. is different from **A**. See text for details.

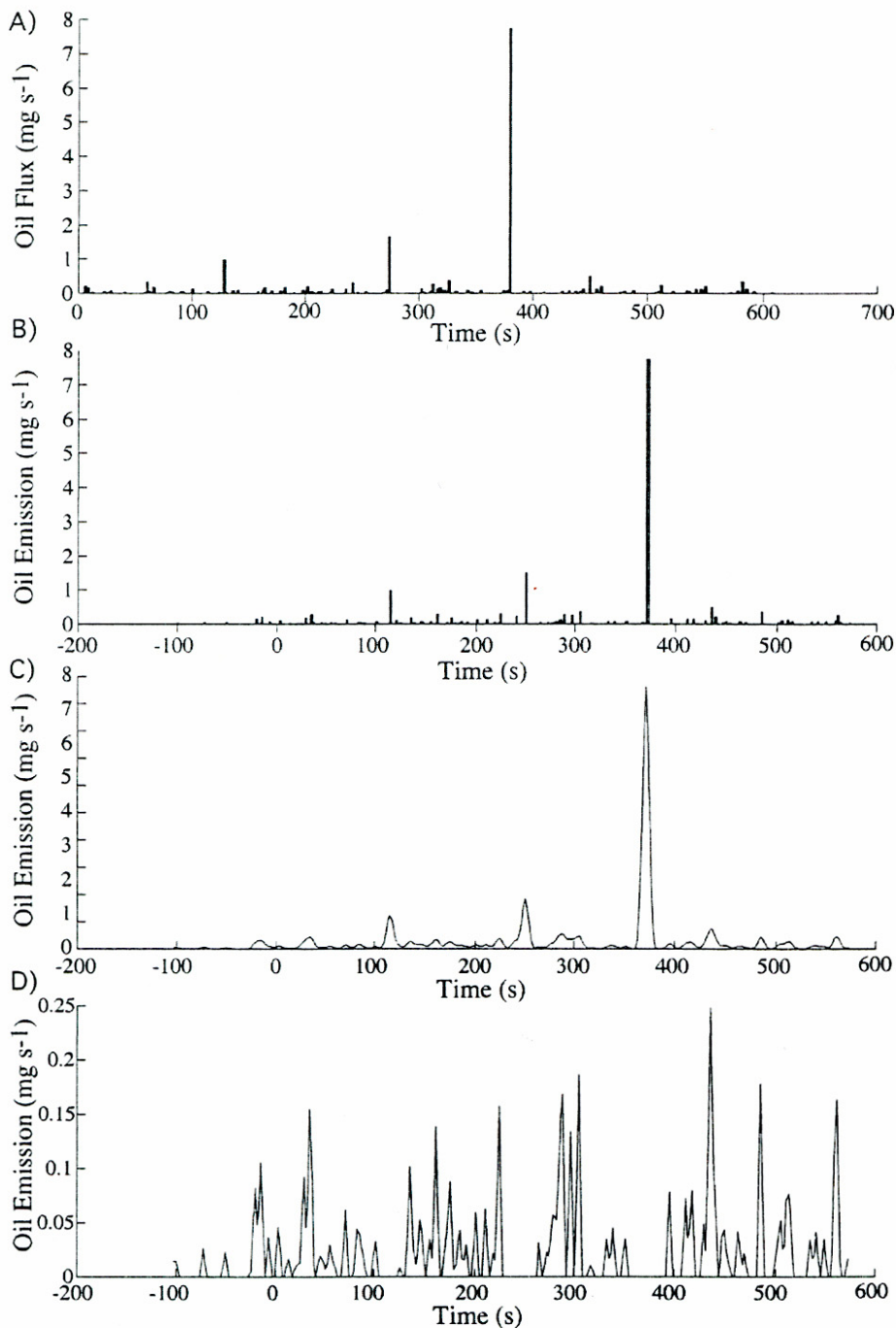
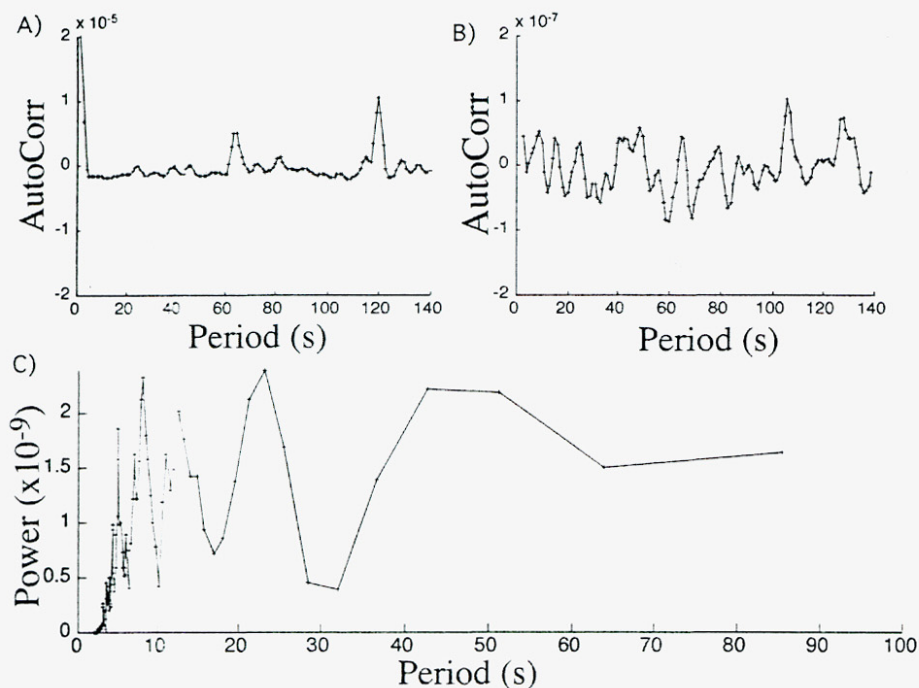


FIGURE 9

A) Autocorrelation (AutoCorr) of time series shown in Fig. 8C and B) with main 3 peaks removed, i.e., of time series shown in Fig. 8D. C) Spectrum of time series with main 3 peaks removed i.e., time series shown in Fig. 8D.



5.0. Discussion

Results (Table 1) were consistent with a tidal influence causing the observed 10-fold increase in both the oil and gas emissions for the last collected sample ~1 hour before the lowest low tide (Fig. 5). Although the increase could have been random, review of the video did not show any indication it was due to a large oil pulse. Unfortunately, data collection for Site 3 covered only a 3.5-hour period approaching the lowest low-tide of a 'minus' tidal cycle (Fig. 5) and did not continue through the oil emission peak. Safety concerns due to an absence of shipboard lighting forced tent retrieval before sunset.

The spectral analysis suggested a swell-induced variation. There are several potential mechanisms by which swell may influence oil and gas emissions at the seabed. One is that the decreasing hydrostatic pressure causes a greater probability that a bubble will escape. This was observed by Leifer and Boles (2004b) at natural hydrocarbon seeps in the Coal Oil Point seep field where the seeps studied were predominantly gas, unlike those observed in the Summerland area. However, swells at Summerland during tent deploy-

ment were extremely small (0.1 - 0.2 m in height). A second mechanism is that the swell-induced surge made bubble formation easier. This mechanism is observed in the laboratory for non-oily bubbles (Tsuge et al., 1981). A third potential mechanism is that slightly negatively buoyant oily bubbles remain in seabed depressions until decreasing hydrostatic pressure from the falling tide makes them buoyant. Since the oil is positively buoyant (0.975 g cm^{-3}), oily bubbles and even pure oil droplets must rise in seawater. Thus, oil droplets and/or oily bubbles that do not rise must contain a small fraction of denser material, such as tar, sediment, or sand. However, analysis of the collected oil did not show significant sand or sediment, thus if the bubbles collected had been resuspended, their initial negative buoyancy must have been due to tar.

6.0. Conclusion

In this study, a video-based seep-tent for quantifying oil and gas emissions from natural seeps and leaking oil facilities was deployed. Video analysis, calibrated with collected and analyzed oil samples allowed a detailed time series of emission rates to be determined for investigation of sources of variability. Oil emission variations with a periodicity comparable to the swell were observed, as was a strong response at 120 s. Improvements in the imaging are necessary to allow more automated analysis.

Acknowledgement

The authors would like to thank the numerous scientists who participated in the field missions: Robin Lewis and John Tarpley, Department of Fish and Game, Oil Spill Prevention and Response (OSPR); Ann Bull, United States Minerals Management Service; and Greg Sanders, United States Fish and Wildlife Service including students Tonya Del Sontro and Una Matko who aided in the construction, testing, and deployment of the large oil seep-tent. We would like to thank the support of the California Department of Fish and Game, OSPR, and the University of California Energy Institute #SB020003. Views and conclusions in this document are those of the authors and should not be interpreted as necessarily representing the official policies, either expressed or implied, of the California government or University of California, Santa Barbara.

References

- Blanchard, D.C. and L.D. Syzdek. 1977. Production of air bubbles of a specified size. *Chem Eng Sci.* 32:1109-1112.
- Clift, R., J.R. Grace and M.E. Weber. 1978. *Bubbles Drops and Particles*. New York: Academic Press. 380 pp.
- Curran, Steve. 1995. Summerland Oil Well Abandonments – Re-evaluation. Internal memorandum to Greg Scott, Mineral Resources Management Division, State Lands Commission. Dated 16 March, 1995. Attachments: Summerland Map, PENCO proposal, Coast Guard Update. Unpublished.
- Fairweather Pacific LLC. 2000. Summerland Well Research Phase 1 Project Report. Unpublished.
- Freckman, J.T. 1981. Memorandum to D.J. Everitts, Chief State Lands Commission. Dated 8 April 1981. Subject Pete Brumis Contract: Oil Seep Location and Containment, Summerland Beach Area, Santa Barbara County.
- Giallonardo, T., A. Koller. 1978. Gaviota offshore gas field. Calif Div of Oil and Gas. Pub No. TR21. 8.
- Golder Assoc, 1995. Map and Dive Report. Geophysical interpretation magnetometer, side-scan sonar, and sub-bottom profiler data, Maps 1 and 2. Report to PENCO/Margeophys CA. Dated Feb.17, 1995. Unpublished.
- Grosbard, A. 2002. Treadwell wharf in the Summerland, California oil field: the first sea wells in petroleum exploration. In: *Oil Industry History*, ed. Friedman. Drake Well Found. 3(1)18.
- Johnson, B.D. and R.C. Cooke. 1979. Bubble populations and spectra in coastal waters: a photographic approach. *J Geophys Res.* 92C2:3761-3766.
- Lammers, D.A. 1975. Internal memorandum to D.J. Everitts. Removal of hazardous conditions, Summerland and Ellwood. Dated July 21, 1975.
- Leifer, I., K. Wilson, J. Tarpley, R. Lewis, R. Imai, M. Sowby, K. Mayer, and C. Moore, 2004. Factors affecting marine hydrocarbon emissions in an area of natural seeps and abandoned oil wells - Summerland, California. Proc. International Oil Spill Conference, Miami, May 2005. Submitted.
- Leifer, I. and Boles. J. 2004a. Measurement of hydrocarbon flow through fractured rock and unconsolidated sediment of a marine seep. *Mar Petrol Geol.* In press.
- Leifer, I. and Boles. J. 2004b. Turbine seep-tent measurements of marine hydrocarbon seep forcing on second time scales. *J Geophys Res.* In press.
- Leifer, I., G. De Leeuw and L.H. Cohen. 2003a. Optical measurement of bubbles: System, design and application. *J Atm Ocean Tech.* 20:1317-1332.
- Leifer, I., G. De Leeuw, L.H. Cohen and G. Kunz. 2003b. Calibrating optical bubble size by the displaced mass method. *Chem Eng Sci.* 58:5211-5216.
- Leifer, I., I. MacDonald. 2003. Dynamics of the gas flux from shallow gas hydrate deposits: Interaction between oily hydrate bubbles and the oceanic environment. *Earth Plan Sci Lett.* 210:411-424.
- Leifer, I. and R. Patro. 2002. The bubble mechanism for transport of methane from the shallow sea bed to the surface: A review and sensitivity study. *Cont. Shelf Res.* 22: 2409-2428.
- National Institute of Health, 2003, NIH Image Software, NIH Image ver. 1.63 (developed at the U.S. National Institutes of Health and available on the Internet at <http://rsb.info.nih.gov/nih-image/>).
- National Research Council (NRC), 2003. *Oil in the Sea III: Inputs and Fates*. Washington, DC: National Academies Press. ISBN 0-309-08438-5, 265 pp.
- Patro, R., I. Leifer and P. Bowyer. 2002. Better bubble process modeling: Improved bubble hydrodynamics parameterisation. In: *Gas Transfer and Water Surfaces*, eds. M. Donelan, W. Drennan, E.S. Salzman and R. Wanninkhof. pp. 315-320, AGU Monograph Volume 127.
- PENCO (Pacific Environmental Corporation). 1995. Golder Assoc., David Evans Assoc. Dive Report, Geophysical survey, magnetometer, side-scan sonar, and sub-bottom profiler data – Maps 1 and 2. Dated Feb 17, 1995. Unpublished.
- Sam, A., C.O. Gomez and J.A. Finch. 1996. Axial velocity profiles of single bubbles in water/froth. *Int. J Min Proc.* 47:177-196.
- Tsuge, H, S. Hibino and U. Nojima. 1981. Volume of a bubble formed at a single submerged orifice in a flowing liquid. *Internat. Chem Eng.* 21:630-636.
- U.S. Coast Guard, (USCG). 1995. Summerland Beach oil well abandonment. Letter from Captain E.E Page to interested parties. Dated 24 Feb. 1995. Unpublished.